Slow quenches in two-dimensional time-reversal symmetric $\mathbb{Z}_2$ topological insulators

Lara Ulčakar[*]

Jozef Stefan Institute, Jamova 39, Ljubljana, Slovenia

Jernej Mravlje, Anton Ramšak, and Tomaž Rejec

Jozef Stefan Institute, Jamova 39, Ljubljana, Slovenia
and Faculty for Mathematics and Physics, University of Ljubljana, Jadranska 19, Ljubljana, Slovenia

We study the topological properties and transport in the Bernevig-Hughes-Zhang model undergoing a slow quench between different topological regimes. Due to the closing of the band gap during the quench, the system ends up in an excited state. We prove that for quenches that preserve the time-reversal symmetry, the $\mathbb{Z}_2$ invariant remains equal to the one evaluated in the initial state. On the other hand, the bulk spin Hall conductivity does change, and its time average approaches that of the ground state of the final Hamiltonian. The deviations from the ground-state spin Hall conductivity as a function of the quench time follow the Kibble-Zurek scaling. We also consider the breaking of the time-reversal symmetry, which restores the correspondence between the bulk invariant and the transport properties after the quench.

I. INTRODUCTION

Topological insulators have been one of the focal points of condensed-matter physics for the past decade due to their interesting properties and potential future applications in nanoelectronics [1–5]. The topological insulators are bulk insulators that at the edges host gapless conducting states which avoid dissipation [6–9]. Although the ground-state physics of topological insulators is already well established, less is known about their response to the time-dependent driving, which is the subject of an active current investigation.

Recently, the question of the response due to the changes in system's parameters (quantum quench) was explored in Chern insulators. Their topological phase is characterized by a nontrivial Chern number and the quantum Hall effect. By definition, the topological invariants are conserved by any adiabatic evolution. But, strikingly, a stronger statement holds. The Chern number is conserved for an arbitrary evolution (the only restriction that the Hamiltonian is smooth in momentum) even if during the evolution the band gap closes [10,11]. Several works [12–17] investigated response due to a rapid change in parameters (i.e., a sudden quench) and found that the bulk Hall response, in contrast to the Chern number, evolves in time. References [18–20] studied a different case in which the parameters are varied slowly between different topological regimes (i.e., a slow quench). The subtle point is that, even though the change in parameters is slow, it can never be adiabatic as the band gap closes. For slow quenches, the bulk Hall response of the postquench system was found to approach the value determined by the topological invariant of the ground state of the final Hamiltonian. In a more general setting, the

response due to slow quenches was also studied in topological superconductors [10,21–23].

Topological systems are gapless at the critical point between different topological regimes, thus even slow quenches between different topological regimes create excitations. The Kibble-Zurek argument [24,25] predicts that the density of excitations scales with the quench time to the power given by the critical exponents, associated with the critical point across which the system is quenched. Agreement of the Kibble-Zurek scaling and the actual response of the bulk after the quench was shown in Refs. [26,27] for Chern insulators and in Ref. [21] for one-dimensional superconductors.

It is natural to ask whether the above findings are general and apply to other types of topological insulators. We consider two-dimensional topological insulators with the time-reversal symmetry (TRS). They are characterized by the $\mathbb{Z}_2$ topological invariant and, in the topological phase, exhibit the spin Hall effect. Importantly, several experimental realizations of these systems exist [28–33].

In this paper we study the topological invariant and the spin Hall effect of the Bernevig-Hughes-Zhang (BHZ) model. We set the system to the ground state of the Hamiltonian in a certain topological regime and then slowly quench the Hamiltonian to a different topological regime. Similar to the case of Chern insulators, the numerical results show that the topological invariant does not change provided the time-reversal symmetry is respected during the quench. We also offer an analytical proof of this finding. In contrast to the $\mathbb{Z}_2$ invariant, the bulk spin Hall conductivity does evolve and, in the limit of an infinitely slow quench, it approaches the value characteristic of the ground state of the final Hamiltonian. We show that the deviations from the ground-state value obey the Kibble-Zurek scaling. We also explore quenches that break the TRS and keep the band gap open at all times (such quenches cannot be realized for Chern insulators). In this case the correspondence

---
[*]lara.ulcakar@ijs.si

is restored: The topological invariant of the system and the spin Hall response are both characteristic of the ones evaluated for the ground state of the final Hamiltonian.

The paper is structured as follows. In Sec. II we introduce the BHZ model and describe how we evaluate the $\mathbb{Z}_2$ invariant and the spin Hall conductivity. Section III is dedicated to the results: The phase diagram of the BHZ model is explored, and the response of the system after a TRS-preserving quench as well as a TRS-breaking quench are shown. In Sec. IV our findings are summarized. In Appendix A, band dispersions and postquench occupancies are analytically discussed. We show the spin Berry curvature [34] and analyze the deviation of the postquench spin Hall conductivity from the ground-state value in detail. We also calculate the critical exponents of the BHZ model. In Appendix B we generalize the proof of the conservation of the Chern number to the case of multiple-band systems, and we give a proof of the conservation of the $\mathbb{Z}_2$ invariant. We present the full formula for the spin Hall conductivity, and we discuss the oscillations of the spin Hall response of the postquench system in Appendix C.

II. MODEL AND METHODS

We study a two-dimensional time-reversal symmetric $s = 1/2$ system on a square crystalline lattice with two orbitals per unit cell. Its bulk momentum-space Hamiltonian is given by

$$\hat{H}(\mathbf{k}) = \hat{s}_0 \otimes [(u + \cos k_x + \cos k_y)\hat{\sigma}_z + \sin k_y \hat{\sigma}_y]$$
$$+ \hat{s}_z \otimes \sin k_x \hat{\sigma}_x + c\, \hat{s}_x \otimes \hat{\sigma}_y, \quad (1)$$

where $\hat{s}_i$ and $\hat{\sigma}_i$ for $i \in \{x, y, z\}$ are Pauli operators, $\hat{s}_0$ and $\hat{\sigma}_0$ are identity operators in spin space and local orbital space, respectively, and $\mathbf{k}$ is an element of the first Brillouin zone (BZ). $c \in \mathbb{R}$ is the coupling constant between spin and orbital degrees of freedom, and u is the staggered orbital binding energy. The Hamiltonian is expressed in the units of intercell hopping amplitude which is equal in both x and y directions. We also set $\hbar$ and the lattice constant to 1. The system has the TRS with the time-reversal operator $\hat{\mathcal{T}} = i\hat{s}_y K$, K being the complex conjugation. When $c = 0$, the original BHZ model [28] is recovered in which the perpendicular projection of the spin s_z is conserved. It describes the low-energy physics of the HgTe/CdTe quantum wells. In systems with band inversion asymmetry and structural inversion asymmetry, such as InAs/GaSb/AlSb type-II semiconductor quantum wells [30], terms that couple states with opposite spin projections and preserve the TRS arise. We model such terms with the simplified $c \neq 0$ term. We consider half-filled systems at zero temperature, meaning that before the quench the lower two energy bands are occupied and the upper two are empty.

We describe the time-reversal symmetric insulator by a set of occupied states $\{|u_n(\mathbf{k})\rangle, \mathbf{k} \in \mathrm{BZ}, 1 \leqslant n \leqslant N_F\}$. A phase of the bulk time-reversal symmetric insulator is characterized by the $\mathbb{Z}_2$ invariant N_{bulk} that distinguishes between the topological regime ($N_{\mathrm{bulk}} = 1$) and the trivial band insulator regime ($N_{\mathrm{bulk}} = 0$). In numerical evaluation it is convenient to use a gauge invariant definition of the $\mathbb{Z}_2$ invariant N_{bulk}: It is equal to the parity of the number of times the Wannier center flow $\theta_n(k_y)$, in range $k_y \in (0, \pi)$, crosses an arbitrarily chosen

fixed value of $\tilde{\theta} \in [-\pi, \pi)$ [35],

$$N_n(\tilde{\theta}) = \text{number of solutions } k_y \in (0, \pi) \text{ of } \theta_n(k_y) = \tilde{\theta}, \quad (2)$$

$$N_{\mathrm{bulk}} = \left(\sum_{n=1}^{N_F} N_n(\tilde{\theta}) \right) \bmod 2. \quad (3)$$

The Wannier center flow $\theta_n(k_y)$ is equal to the phase of the nth eigenvalue of the Wilson loop, a multiband generalization of the Berry phase. The Wilson loop is defined as

$$W(k_y) = M^{(12)} M^{(23)} \cdots M^{(N-1,N)} M^{(N,1)}, \quad (4)$$

$$M_{nm}^{(kl)} = \langle u_n(k\delta_k - \pi, k_y) | u_m(l\delta_k - \pi, k_y) \rangle, \quad (5)$$

where $\delta_k = 2\pi/N$ is the discretization step in the momentum space of a lattice with periodic boundary conditions and $N \times N$ sites. Matrices $W(k_y)$ and $M^{(kl)}$ are of dimension $N_F \times N_F$. Wannier center flow can be associated with the expectation value of the relative position of a state from the nearest lattice site. The $\mathbb{Z}_2$ invariant is well defined only for systems with TRS in which the Wannier center flow is symmetric about and doubly degenerate at $k_y = 0, \pi$. For pedagogical discussion see Ref. [36].

We evaluate the spin Hall conductivity $\sigma_{xy}^{\mathrm{spin}}$ by calculating the spin current density j_y^{spin} as a response to an electric field E_x in the perpendicular direction. For the spin current defined as [34,37] (see Refs. [38–40] for other possible definitions)

$$\hat{j}_y^{\mathrm{spin}} = \frac{1}{2} \frac{1}{N^2} \hat{s}_z \frac{\partial \hat{H}(\mathbf{k})}{\partial k_y}, \quad (6)$$

the spin Hall conductivity can be evaluated as

$$\sigma_{xy}^{\mathrm{spin}} = \frac{1}{E_x} \sum_{n=1}^{N_F} \sum_{\mathbf{k}} \langle u_n(\mathbf{k}) | \hat{j}_y^{\mathrm{spin}} | u_n(\mathbf{k}) \rangle. \quad (7)$$

E_x is a small homogeneous electric field switched on at $t = t_E$, $E_x(t) = E_0 \{1 - \exp[-(t - t_E)/\tau_E]\}$. Throughout the paper we choose $\tau_E = 10$, $E_0 = 0.0001$, and the system size 200×200. We checked that increasing the system size further does not affect the results presented in the paper. To preserve the translational symmetry we introduce the electric field through a spatially homogeneous time-dependent vector potential $A_x(t) = -\int E_x(t) dt$ [40].

III. RESULTS

A. Phase diagram of the BHZ model

The phase diagram of the BHZ model, shown in Fig. 1(a), describes the topological phase of the ground state of the Hamiltonian (1) at parameters $P = (u, c)$. It consists of three insulating regions: the trivial regime with $N_{\mathrm{bulk}} = 0$ (white) and two topological regimes with $N_{\mathrm{bulk}} = 1$ (gray). Insulating regimes are separated from each other by a broad Dirac semimetal regime (DSM) in which the system has a closed band gap with linear dispersion. The upper boundary between the semimetal and the trivial insulator regimes is $c(u) = \sqrt{2 - u^2/2}$, whereas the lower boundaries between the topological insulator and the semimetal regimes are $c(u) = \sqrt{1 - (u - 1)^2}$ and $c(u) = \sqrt{1 - (u + 1)^2}$. In the semimetal
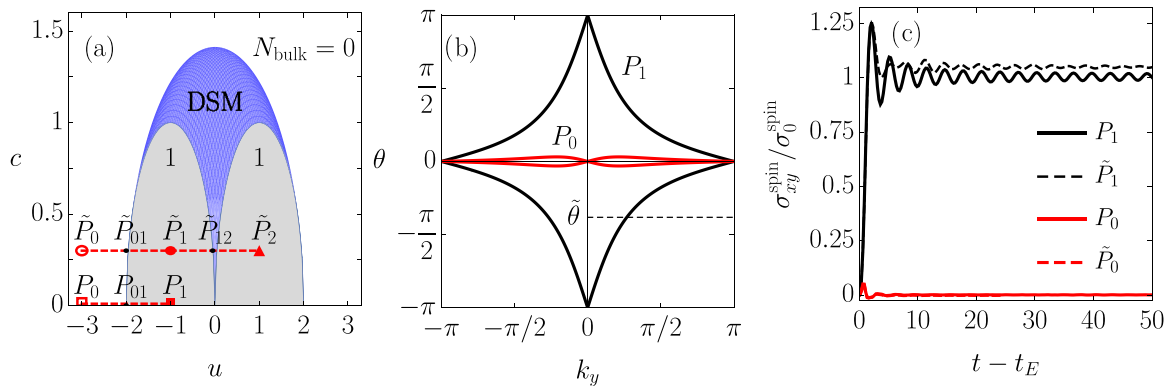
FIG. 1. (a) Phase diagram of the BHZ model in $P = (u,c)$ parameter space. The gray colored area marks topological insulator parameter regimes where $N_{bulk} = 1$, the white area marks the trivial insulator regime with $N_{bulk} = 0$, and the blue area marks the Dirac semimetal regime. Points $P_0 = (-3,0)$, $\tilde{P}_0 = (-3,0.3)$, $P_1 = (-1,0)$, $\tilde{P}_1 = (-1,0.3)$, and $\tilde{P}_2 = (1,0.3)$ mark initial and final points between which parameters of the Hamiltonian are quenched (dashed). Several band gap closing points are marked as P_{01}, $\tilde{P}_{01}$, and $\tilde{P}_{12}$. (b) Wannier center flows for the ground state of the Hamiltonian at P_0 and P_1. The dashed black line presents a chosen $\tilde{\theta}$ used for the determination of the $\mathbb{Z}_2$ invariant. (c) Spin Hall conductivities at P_0, $\tilde{P}_0$, P_1, and $\tilde{P}_1$, where $\sigma_0^{spin} = e/2\pi$.

regime the band gap closes at different points in the Brillouin zone, in particular, for $P_{01} = (-2,0)$ at the Γ point at $\mathbf{k} = (0,0)$, for $P = (0,0)$ at $\mathbf{k} = (0,\pi)$ and $(\pi,0)$, for $P = (2,0)$ at $\mathbf{k} = (\pi,\pi)$, and for $P = (\pm 1,1)$ at $\mathbf{k} = (\pm\pi/2,0)$ and $(0, \pm \pi/2)$. In Appendix A, analytical expressions for the band dispersions near the band-gap closing are given, and graphs are shown at the band-gap closing points P_{01}, $\tilde{P}_{01}$, and $\tilde{P}_{12}$.

For the purpose of later comparison with the response after the quench, we first establish what kind of behavior to expect in distinct parameter regions for the ground state. Figure 1(b) shows Wannier center flows $\theta(k_y)$ at P_0 and P_1 whereas the dashed line is an arbitrary $\tilde{\theta}$ chosen to evaluate the Eq. (3). For instance, one can see that in the ground state at P_1 the Wannier center flow crosses the dashed line once, hence P_1 corresponds to the topological regime.

The spin Hall conductivity evaluated as described in Eq. (7) is presented in Fig. 1(c). One can see a sharp distinction between the results in the topological regime (P_1 and $\tilde{P}_1$) where, following a steep rise, the spin Hall conductivity oscillates around a finite value and the trivial regime (P_0 and $\tilde{P}_0$) where it oscillates around zero instead. The frequency of these oscillations is equal to the band gap. The amplitude of the oscillations diminishes with time, and it becomes smaller if the electric field is turned on more adiabatically (i.e., with longer τ_E). In the topological regime, the ground-state value of the spin Hall conductivity is quantized in the units of $\sigma_0^{spin} = e/2\pi$ (e is the charge of electric carriers) whenever s_z is conserved (e.g., in P_1 it is equal to σ_0^{spin}) but has a nonquantized value elsewhere [9]. In contrast to the spin Hall conductivity, the Hall conductivity vanishes in all parameter regimes due to the TRS.

So far we have analyzed the phase diagram in the $u < 0$, $c > 0$ region. As shown in Appendix A, the Hamiltonian possesses certain symmetries which relate phases in the remaining regions of the phase diagram to those in the $u < 0$, $c > 0$ region. Upon changing the sign of u, the $\mathbb{Z}_2$ invariant is preserved while the spin Hall conductivity changes sign. The spin Hall conductivity in $\tilde{P}_2$ is thus the negative of that in $\tilde{P}_1$. Upon changing the sign of c, both the $\mathbb{Z}_2$ invariant and the spin Hall conductivity remain unchanged.

B. Slow quenches with preserved TRS

Now we turn to the discussion of quenches. We studied the response of the system undergoing a slow quench of the parameters of the Hamiltonian between different topological regimes, indicated by the dashed lines in Fig. 1(a). The parameter u is changed smoothly as $u(t) = u_0 + (u_1 - u_0)\sin^2(\frac{\pi}{2}t/\tau_u)$ for $t \in [0,\tau_u]$. For times $t > \tau_u$, u has a constant value of u_1. This unitary evolution does not break the TRS, namely, during the quench the Hamiltonian stays time-reversal symmetric.

We first discuss the $c = 0$ case. In Fig. 2(a) the Wannier center flows are shown at different times during the quench $P_0 \to P_1$ with $\tau_u = 15$. The system starts in the trivial phase with the shape of the Wannier center flow as in Fig. 1(b) (see P_0). With progressing time, the Wannier center flow evolves into the diamond-shape characteristic of the ground state at P_1 (dashed) for $|k_y|$ larger than a certain k_0 but deviates from that for $|k_y| < k_0$. Since the Wannier center flow vanishes at $k_y = 0$ for all times, the $\mathbb{Z}_2$ invariant remains unchanged. We also derived this analytically and give the corresponding proof for a general TRS-preserving unitary evolution in Appendix B.

The shape of the Wannier center flow can be related to the band occupancy shown in Fig. 2(b). The population of the (doubly degenerate) lowest-energy-level $n_1(0,k_y)$ after the quench is shown for several quench times τ_u. The population of the lowest-energy level drops at small $|\mathbf{k}| < k_0$ and vanishes at the Γ point where the band gap closes during the quench. The final occupancies can also be derived analytically using the Landau-Zener formula [41] which gives $n_1(\mathbf{k}) = 1 - \exp[-\pi k^2/v_u]$, $v_u = |\frac{du}{dt}|_{t=\tau_u/2}| = \pi|u_1 - u_0|/2\tau_u$, and consequently the delimiting $k_0 \sim \sqrt{1/\tau_u}$ (see Appendix A). The distance from the Γ point thus determines how close the final state is to the ground state of the final Hamiltonian (at the corresponding $\mathbf{k}$), which explains the shape of the Wannier flows.

Figure 2(c) shows the k points at which the band gap closes during the considered quenches. In contrast to the $P_0 \to P_1$ quench where the band gap closes at P_{01} at an isolated point, for the $\tilde{P}_0 \to \tilde{P}_1$ quench, the band gap closes at parameters
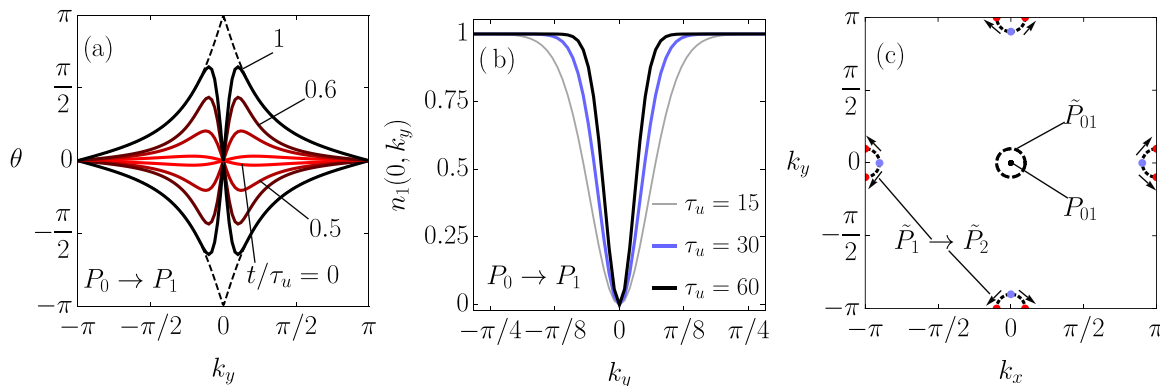
FIG. 2. (a) Wannier center flows of the ground state at P_1 (black, dashed) and of nonequilibrium states (solid lines) at various times during the quench from P_0 to P_1 with $\tau_u = 15$. (b) Population of the first energy level after the $P_0 \rightarrow P_1$ quench. (c) Band-gap closing in k space. For $P_0 \rightarrow P_1$ and $\tilde{P}_0 \rightarrow \tilde{P}_1$ quenches the band gap closes at P_{01} and $\tilde{P}_{01}$, respectively. However, for the $\tilde{P}_1 \rightarrow \tilde{P}_2$ quench, it closes gradually starting at the blue points and moving to the red ones as indicated with arrows.

$\tilde{P}_{01}$ on a circle around the Γ point. The quench $\tilde{P}_1 \rightarrow \tilde{P}_2$ is distinct from the former two as parameters of the Hamiltonian enter the conducting region [see Fig. 1(a)], and the band gap remains closed in a range of parameter values near $u = 0$. On entering the conducting region at $\tilde{P}_{12}$, the band gap closes at four points [blue points in Fig. 2(c)] which with increasing u split into eight points that with the progressing quench move along circles centered at momenta $(\pm \pi, 0)$ and $(0, \pm \pi)$. When they reach the Brillouin-zone boundary [red points in Fig. 2(c)], the band gap opens, and the insulating topological regime is reached.

After the quench with $0 < c \ll 1$, the electrons with momenta close to those on a circle where the band gap closes during the quench are excited to the lower conduction band with probability $\exp[-\pi(|\mathbf{k} - \mathbf{k}_c| - c)^2/v_u]$, where $\mathbf{k}_c$ is the center of the circle. At momenta on the circle the population of the conduction band is 1. Correspondingly, the Wannier center flow is deformed, and the topological invariant remains equal to that of the initial state.

The total number of excitations is $N_{exc} = |u_1 - u_0|/8\pi\tau_u$ for systems with $c = 0$ and $N_{exc} = c\sqrt{|u_1 - u_0|/8\pi\tau_u}$ for systems with $0 < c \ll 1$, i.e., in systems with zero and nonzero c's it scales differently with τ_u. As u is a linear function of time near the gap closing at $t = \tau_u/2$, we can compare these results to the predictions of the Kibble-Zurek scaling for linear quenches with a fixed rate $N_{exc} \propto \tau_u^{-\nu d/(\nu z + 1)}$. Here, d is the spatial dimension whereas ν and z are the correlation length and the dynamical critical exponent, respectively, associated

with the critical point across which the system is quenched. Following Ref. [42] (see Appendix A), we obtained the critical exponents of the BHZ model. These give the same behavior as found from the Landau-Zener formula and read $\nu = 1$ and $z = 1$ for $c = 0$ and $\nu = 1/2$ and $z = 2$ for $0 < c \ll 1$. Systems with zero and nonzero c's thus belong to different universality classes.

Spin Hall conductivities, evaluated as the electric field is turned on after the quench, are for several quench durations shown in Fig. 3(a). As for systems in the ground state, the spin Hall conductivity first experiences transient behavior and then oscillates around a nonzero value $\bar{\sigma}_{xy}^{\text{spin}}$ with the frequency equal to the band gap of the final Hamiltonian. As seen in the plot and as discussed in more detail below, the oscillations become small for slow enough quenches. Importantly, in contrast to the unchanged $\mathbb{Z}_2$ invariant, $\bar{\sigma}_{xy}^{\text{spin}}$ approaches the value characteristic of the final Hamiltonian. This generalizes the corresponding findings in Chern insulators in Ref. [18].

The dependence of $\bar{\sigma}_{xy}^{\text{spin}}$ on the quench duration τ_u is presented in Fig. 3(b) for several quenches. The deviations from the ground-state values vanish for quenches slow enough. In order to understand the observed behavior, we evaluated the spin Hall conductivity using the time-dependent perturbation theory (following the discussion for Chern insulators in Ref. [13], see also Appendix C). We obtain the following analytical formula for the time-averaged spin Hall conductivity at long times:

$$\bar{\sigma}_{xy}^{\text{spin}} = \frac{e}{(2\pi)^2} \sum_{n=1}^{2N_F} \int d\mathbf{k} \, n_n(\mathbf{k}) \Omega_n^{\text{spin}}(\mathbf{k}), \tag{8}$$

$$\Omega_n^{\text{spin}}(\mathbf{k}) = -2 \, \text{Im} \sum_{\substack{m=1 \\ m \neq n}}^{2N_F} \frac{\langle u_n(\mathbf{k})| \frac{1}{2}\hat{s}_z \partial_{k_y} \hat{H}(\mathbf{k})|u_m(\mathbf{k})\rangle \langle u_m(\mathbf{k})|\partial_{k_x} \hat{H}(\mathbf{k})|u_n(\mathbf{k})\rangle}{[E_n(\mathbf{k}) - E_m(\mathbf{k})]^2}, \tag{9}$$

where $n_n(\mathbf{k})$ is the occupation of the nth energy band at $\mathbf{k}$ with eigenenergy $E_n(\mathbf{k})$. The spin Hall conductivity is expressed as an integral of the spin Berry curvature $\Omega_n^{\text{spin}}(\mathbf{k})$ [34] weighted

by the band occupancy. The spin Berry curvature of conduction bands has the opposite sign to that of the valence bands. Therefore, the excitations above the ground state diminish
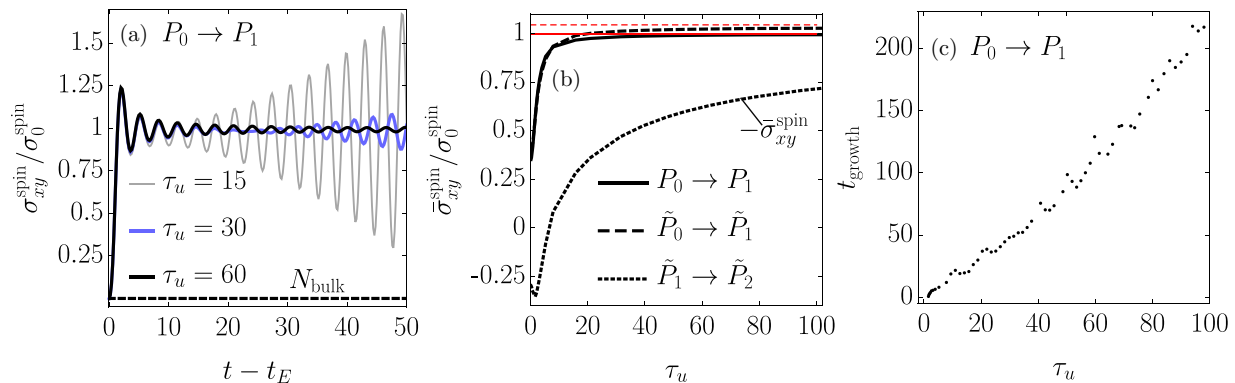
FIG. 3. (a) Topological invariant (dashed) and the spin Hall conductivity (solid lines) of the nonequilibrium states, resulting from the quench from P_0 to P_1. (b) Time-averaged spin Hall conductivity after the $P_0 \to P_1$ quench (solid) converges for $\tau_u \to \infty$ to the ground-state value of $\hat{H}(P_1)$ (thin, solid) and for systems after the $\tilde{P}_0 \to \tilde{P}_1$ (dashed) to the ground-state value of $\hat{H}(\tilde{P}_1)$ (thin, dashed). Time-averaged spin Hall conductivity after the $\tilde{P}_1 \to \tilde{P}_2$ quench (dotted) is multiplied by a factor of -1 and converges to the ground-state value of $\hat{H}(\tilde{P}_2)$. (c) Time at which the amplitude of oscillations in the spin Hall response after the quench $P_0 \to P_1$ increases for 10% above the minimal amplitude.

the time-averaged spin Hall conductivity, which explains the dependence seen in Fig. 3(b). For slow quenches excitations occur in a small region in k space and thus contribute little to the integral in Eq. (8). Therefore, the time-averaged conductivity converges for long τ_u to the ground-state one. For systems with $c = 0$ the time-averaged value for slow quenches can be further simplified to $\bar{\sigma}_{xy}^{\mathrm{spin}} \approx \frac{e}{2\pi}(1 - |u_1 - u_0|/4\tau_u)$ where we used the Landau-Zener formula for the energy-band occupancy and approximated the spin Berry curvature with its value at the Γ point (similarly was performed in Ref. [19]). A similar calculation for systems with $c \neq 0$ shows that the deviation of the postquench spin Hall response from the ground-state value diminishes for long quenches as $\delta\sigma_{xy}^{\mathrm{spin}} \propto 1/\sqrt{\tau_u}$. For slow enough quenches $\delta\sigma_{xy}^{\mathrm{spin}}$ is proportional to the total number of excitations and hence obeys the Kibble-Zurek scaling.

The formula Eq. (9) is also useful for discussion of the different magnitudes of the deviations from ground-state values for different quench protocols as seen in Fig. 3(b) (horizontal thin lines denote ground-state values). Namely, after the $\tilde{P}_1 \to \tilde{P}_2$ quench, the response deviates from the ground-state result much more than the responses after the other two quenches. This is due to two facts. First, the number of produced excitations is larger and, second, the excitations occur at momenta where the spin Berry curvature is large (see Appendix A). More precisely, the number of excited electrons is approximately two times larger for $\tilde{P}_1 \to \tilde{P}_2$ than for the $\tilde{P}_0 \to \tilde{P}_1$ quench. The number is roughly given by the length of the circles in Fig. 1(c). During the $\tilde{P}_1 \to \tilde{P}_2$ quench, the band-gap closing points cover two full circles. Second, the value of the spin Berry curvature where those excitations occur is larger for the former quench protocol. For the $P_0 \to P_1$ and the $\tilde{P}_0 \to \tilde{P}_1$ protocols, the spin Berry curvatures are small in the region with excited electrons, hence the deviations from the ground-state value of the spin Hall conductivity are smallest there.

We now consider the oscillations around the time-averaged value. For short times oscillations diminish, and for later times they start to grow quadratically (see Appendix C). The time t_{growth} after which the amplitude of oscillations starts to grow increases with the duration of the quench τ_u. In order to

give a somewhat more quantitative estimate of the behavior, we defined t_{growth} as the time after which the amplitude of the oscillations increases by 10% above the minimal amplitude found for a given τ_u, Fig. 3(c). Note that t_{growth} is roughly linear in τ_u, which means that for slow quenches there is a long time window where these oscillations are not important. In Appendix C, we show that the growth of the oscillations occurs due to the nonzero off-diagonal elements of the density matrix in the basis of the eigenstates of the final Hamiltonian. Actually, often in evaluations of the Hall conductivity [16,43,44] only the diagonal parts of the density matrix are retained, which is supported by the argument that a measurement of the Hall conductance unavoidably introduces decoherence and collapses the quenched state to a state represented by a diagonal ensemble.

C. Slow quenches with symmetry breaking

When an important symmetry associated with a certain class of topological insulators is broken during a quench, different topological regimes can become adiabatically connected [36], i.e., the band gap can remain open everywhere during the quench. The topological invariant becomes ill defined in this case. We study such processes by adding a convenient TRS-breaking term $b\,\hat{s}_x \otimes \hat{\sigma}_x$ to the BHZ model. In parallel to changing the parameter u as in the case of the TRS-preserving quench, the amplitude b is turned on during the quench as $b(t) = b_0 \sin^2(\pi t/\tau_u)$. In this way the Hamiltonian has the TRS before and after the quench, but for $0 < t < \tau_u$ the symmetry is broken and the band gap remains open. When the quench is performed slowly enough compared to the inverse of the minimal band gap during the quench, there are almost no excitations to conduction bands. This can be seen in Fig. 4(a) where the population of the first energy band after the $P_0 \to P_1$ quench is shown for various quench times. In the adiabatic limit, the system ends up in the ground state of the final Hamiltonian and thus in the topological phase with $N_{\mathrm{bulk}} = 1$.

Time-reversal properties of the system during the quench can be observed from the graphs of the Wannier center flow in Fig. 4(b). At $t/\tau_u = 0$ and $t/\tau_u = 1$ the Wannier center flow has the typical form for the trivial and topological phases,
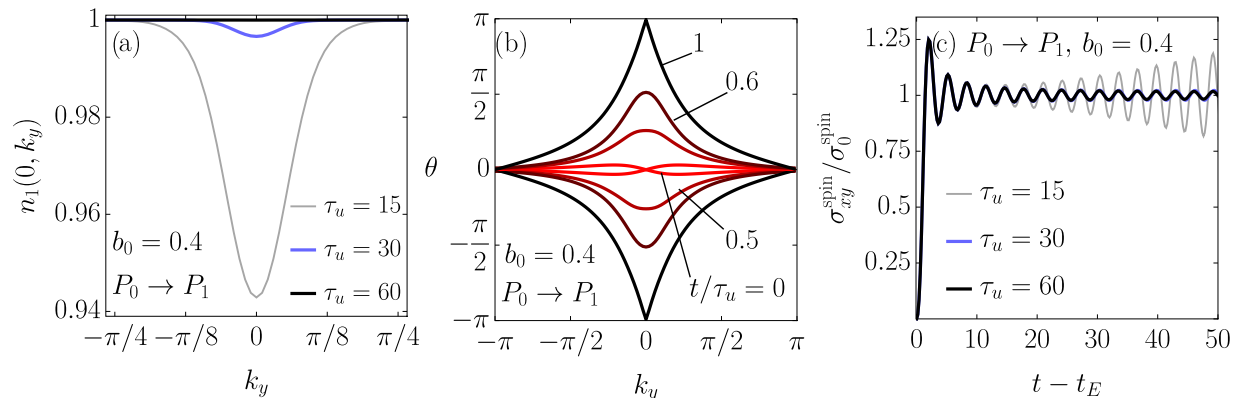
FIG. 4. Properties of the system quenched from P_0 to P_1 with a TRS-breaking term of amplitude $b_0 = 0.4$. (a) Population of the first energy-level $n_1(0, k_y)$ after the quench. (b) Wannier center flows of the nonequilibrium state at different times during the quench with $\tau_u = 15$. (c) Spin Hall conductivity after the quench. The graphs with $\tau_u = 30$ and $\tau_u = 60$ overlap as the quench with such τ_u and b_0 is already adiabatic.

respectively, whereas at $t/\tau_u = 0.5$ and $t/\tau_u = 0.6$ the system does not exhibit the TRS as can be seen by the absence of double degeneracy at $k_y = 0$ and $k_y = \pi$.

After the quench, the electric field is turned on. At long times, the spin Hall response oscillates around a constant value with the frequency equal to the band gap of the final Hamiltonian as shown in Fig. 4(c). For a quench slower than the inverse of the minimal band gap during the quench, the system exhibits ground-state spin Hall response. It also coincides with the spin Hall response of the system after an infinitely slow symmetry-preserving quench. For faster quenches, there are excitations present even in the symmetry-breaking case [see Fig. 4(a)] so the growth of oscillations and the deviation of the time-averaged value from the ground-state value can be observed. However, compared to the case of symmetry-preserving quench, the oscillations are less prominent because of the smaller number of excitations.

IV. CONCLUSIONS

In this paper we calculated the topological invariant and the transport properties of the time-reversal symmetric BHZ model undergoing a slow quench between different topological regimes. Similar to the case of the Chern insulators discussed in the literature earlier, our results show that such a quench preserves the bulk topological invariant. Conversely, the spin Hall response is changed and for slow enough quenches approaches that of the ground state of the final Hamiltonian. The transport properties that are given as an integral over the Brillouin zone can universally be expected to be close to those of the final Hamiltonian ground state as the quench is adiabatic for all states except for those in a small region in the momentum space. Hence, for the cases where the bulk invariant is conserved, the loss of correspondence of the bulk invariant and the bulk transport properties is expected. It would be interesting to explore the behavior of bulk invariants during quenches in other systems, too.

We also considered quenches during which the TRS is broken, which allows the adiabatic connection between different regimes and hence restores the correspondence between the bulk invariant and the transport.

It would be interesting to investigate the dynamics of time-reversal symmetric systems also experimentally with HgTe/CdTe and InAs/GaSb/AlSb type-II semiconductor quantum wells where the quench could perhaps be performed by varying the inversion-breaking electric potential in the z direction, which can be tuned by a top gate in experiments [45–47]. Alternatively, time-dependent Hamiltonians can be also realized in ultracold atoms [48–52].

APPENDIX A: BAND PROPERTIES AT AND AFTER BAND-GAP CLOSING

1. Band-gap closings and postquench occupancies

Let us introduce u_c and $\mathbf{k}_c$ which are the values of u and $\mathbf{k}$, respectively, where the band gap closes along the $c = 0$ line of the phase diagram in Fig. 1(a). For quenches discussed in this paper the relevant band closings are those at $u_c = -2$ [the gap closes at $\mathbf{k}_c = (0,0)$] and at $u_c = 0$ [the gap closes at $\mathbf{k}_c = (\pi,0)$ and at $\mathbf{k}_c = (0,\pi)$]. For systems with $0 < c \ll 1$ ($c = 0.3$ is small enough), the band gap closes at momenta close to those at $c = 0$. Expanding the Hamiltonian (1) to the first order in the deviation of the momentum from $\mathbf{k}_c$ we obtain band dispersions $\pm\sqrt{(q - c)^2 + \delta u^2}$ and $\pm\sqrt{(q + c)^2 + \delta u^2}$, where $q = |\mathbf{k} - \mathbf{k}_c| \ll \pi$ and $\delta u = u - u_c$. For $c = 0$ the band gap between two spin degenerate valence bands and two spin degenerate conduction bands closes at $\mathbf{k}_c$ with linear dispersion $\pm q$ whereas for $0 < c \ll 1$ the band gap between the upper valence band and the lower conduction band closes on a circle with radius c around $\mathbf{k}_c$ again with linear dispersion $\pm|q - c|$. Figure 5 shows cross sections of band dispersions for different k_x's at parameters P for which the band gap closes during quenches discussed in this paper. Note that in the case of the $\tilde{P}_1 \rightarrow \tilde{P}_2$ quench there is a semimetal region of a finite width around $u = 0$ in the phase diagram. Although the band gap closes on a circle as discussed above, for different points along the circle this happens at different values of u inside the
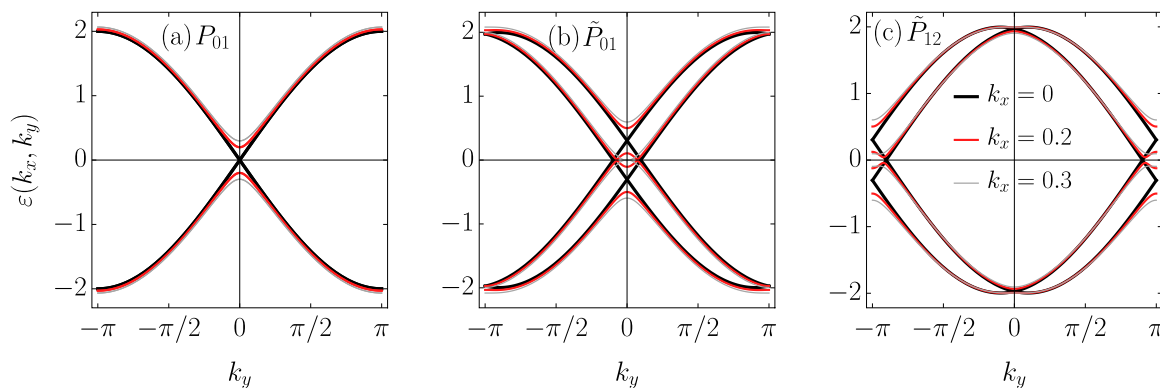
FIG. 5. Band dispersions at (a) P_{01}, (b) $\tilde{P}_{01}$, and (c) $\tilde{P}_{12}$.

semimetal region. For example, for the particular value of u corresponding to Fig. 5(c) the gap is closed only at $k_x = 0$.

Near the band-gap closing, i.e., for $|\delta u| \ll 1$ and $|q - c| \ll 1$, the low-energy physics is described by the Landau-Zener Hamiltonian. The probability for the transition from the valence to the conduction band is given by the Landau-Zener formula $e^{-\pi(q-c)^2/v_u}$, where $v_u = |\frac{du}{dt}|_{u=u_c}|$ [41]. In our case $v_u = \pi|u_1 - u_0|/2\tau_u$. Excitations to the conduction band occur at momenta where $|q - c| \lesssim \sqrt{v_u}$, i.e., on a disk of radius $\sim \sqrt{v_u}$ for $c = 0$ and, provided τ_u is long enough so that $\sqrt{v_u} \ll c$, on a ring of radius c and of width $\sim \sqrt{v_u}$ for $0 < c \ll 1$. Figure 6 shows occupations of the upper valence band after the quenches considered in this paper. As $v_u \propto 1/\tau_u$, the total number of electrons excited to the conduction band around one gap closing N_{exc} is proportional to $1/\tau_u$ for $c = 0$, whereas for $0 < c \ll 1$ it is proportional to $c/\sqrt{\tau_u}$. A more detailed calculation yields $N_{\text{exc}} = |u_1 - u_0|/8\pi\tau_u$ and $N_{\text{exc}} = c\sqrt{|u_1 - u_0|/8\pi\tau_u}$, respectively. Note that for the quench $\tilde{P}_1 \to \tilde{P}_2$ the gap closes on two separate circles and for the quench $P_0 \to P_1$ between two pairs of bands, so the number of excitations is twice as high.

2. Spin Berry curvature and postquench response

An intriguing observation made in Fig. 3(b) is that after the $\tilde{P}_1 \to \tilde{P}_2$ quench, the time-averaged spin Hall conductivity $\bar{\sigma}_{xy}^{\text{spin}}$ deviates from the ground-state value of the final Hamiltonian for an order of magnitude more than after the $\tilde{P}_0 \to \tilde{P}_1$

quench. Here we provide a detailed explanation of this puzzling behavior.

For τ_u large enough, the deviation of the postquench time-averaged spin Hall conductivity from its value in the ground state of the postquench Hamiltonian can be expressed as

$$\delta\bar{\sigma}_{xy}^{\text{spin}} \approx -2e \sum_{\kappa} N_{\text{exc},\kappa} \bar{\Omega}_{2,\kappa}^{\text{spin}}, \tag{A1}$$

where κ runs over the band-gap closings and $\bar{\Omega}_{2,\kappa}^{\text{spin}}$ is the spin Berry curvature of the upper valence band of the final Hamiltonian, averaged over the momenta where the band gap closes for a particular κ. The prefactor 2 comes from the fact that both electrons excited to the conduction band as well as holes left in the valence band contribute equally as the spin Berry curvatures of those bands are opposite $\Omega_3^{\text{spin}}(\mathbf{k}) = -\Omega_2^{\text{spin}}(\mathbf{k})$. Figure 7 shows spin Berry curvatures of the upper valence band of postquench Hamiltonians discussed in this paper. By considering Figs. 6 and 7 it is apparent that excitations to the conduction band after the $\tilde{P}_1 \to \tilde{P}_2$ quench occur at momenta where the spin Berry curvature is for an order of magnitude larger than the spin Berry curvature in the excitation region after the $P_0 \to P_1$ and $\tilde{P}_0 \to \tilde{P}_1$ quenches.

As seen in Figs. 7(b) and 7(c), the spin Berry curvature at $\tilde{P}_2$, when translated by π in both k_x and k_y directions, is the negative of the spin Berry curvature at $\tilde{P}_1$. This is due to the fact that the Hamiltonian at $-u$ can be transformed into that at u: $\hat{s}_y \otimes \hat{\sigma}_x \hat{H}_{-u}(k_x + \pi, k_y + \pi)\hat{s}_y \otimes \hat{\sigma}_x = \hat{H}_u(k_x, k_y)$. A short calculation shows that the spin Hall conductivity of the ground state at $-u$ is of the opposite sign to the one at u whereas the $\mathbb{Z}_2$
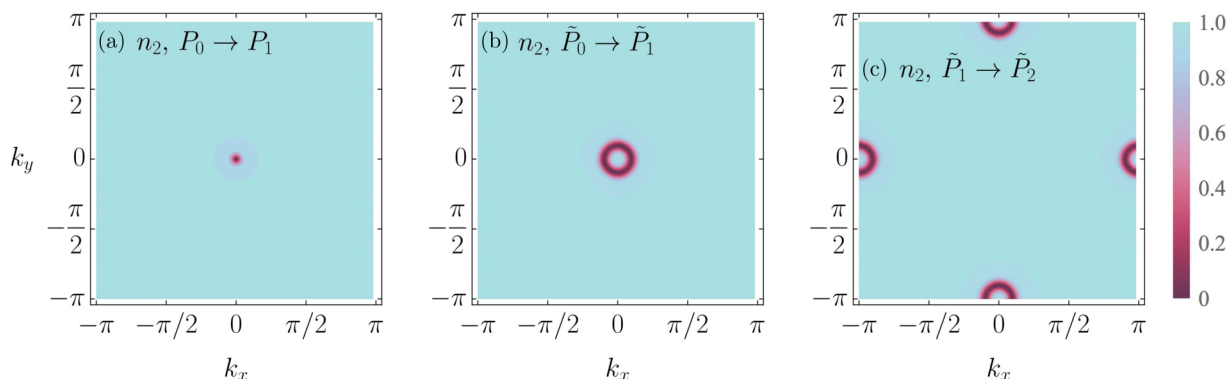
FIG. 6. Occupancy of the upper valence band of the BHZ model quenched among (a) $P_0 \to P_1$, (b) $\tilde{P}_0 \to \tilde{P}_1$, and (c) $\tilde{P}_1 \to \tilde{P}_2$ for $\tau_u = 60$.
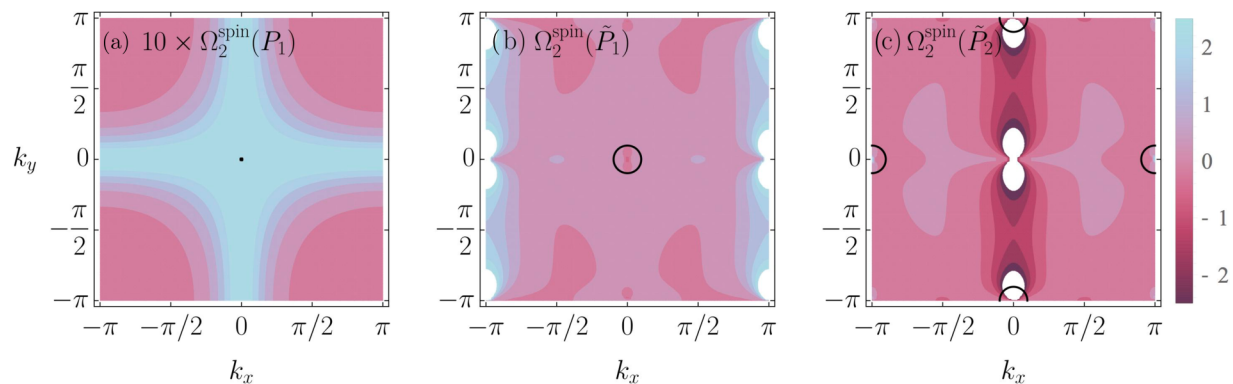
FIG. 7. Spin Berry curvature of the upper valence band of the BHZ model at parameters (a) P_1, (b) $\tilde{P}_1$, and (c) $\tilde{P}_2$. The value of the spin Berry curvature at P_1 is multiplied by 10. Black lines denote momenta at which the band gap closes during quenches (a) $P_0 \to P_1$, (b) $\tilde{P}_0 \to \tilde{P}_1$, and (c) $\tilde{P}_1 \to \tilde{P}_2$. White regions correspond to the values out of the color code scale.

invariant is the same. Similarly, Hamiltonians at $-c$ and c are related as $\hat{s}_z \hat{H}_{-c}(\mathbf{k})\hat{s}_z = \hat{H}_c(\mathbf{k})$. From this it can be shown that the spin Hall conductivity and the $\mathbb{Z}_2$ invariant are the same for the ground state at c and $-c$.

3. Calculation of the critical exponents

Let us choose a control parameter ε such that the system undergoes a quantum phase transition at $\varepsilon = 0$. A quantum phase transition is characterized by the divergence of both the characteristic length-scale $\xi(\varepsilon) \propto |\varepsilon|^{-\nu}$ and characteristic time-scale $\tau(\varepsilon) \propto |\varepsilon|^{-z\nu}$, ν being the correlation length, and z being the dynamical critical exponent. According to the Kibble-Zurek argument, the scaling of the produced defect density, in our case excitations to conduction bands, depends on these critical exponents. In this section, we calculate the critical exponents of the BHZ model.

We extract the critical exponent $z\nu$ from the characteristic time scale, which is the inverse of the band gap. Noting that the spectrum near the gap closing is of the form $\pm\sqrt{(q \pm c)^2 + \delta u^2}$, we find that the minimal gap vanishes as $\delta u^{z\nu} = \delta u$, yielding the critical exponent $z\nu = 1$.

For the calculation of the correlation length critical exponent ν we follow Ref. [42]. Authors of Ref. [42] define the scaling function $F(\mathbf{k}, \varepsilon) = (\hat{\mathbf{k}}_s \cdot \nabla_{\mathbf{k}})^2 \mathrm{Pf}(m)$, where $\hat{\mathbf{k}}_s$ is the scaling direction and m is the matrix of the time-reversal operator $\hat{\mathcal{T}}$ with elements $m_{\alpha\beta}(\mathbf{k}, \varepsilon) = \langle u_\alpha(\mathbf{k}, \varepsilon)|\hat{\mathcal{T}}|u_\beta(\mathbf{k}, \varepsilon)\rangle, |u_\alpha(\mathbf{k}, \varepsilon)\rangle$ being the occupied eigenstate α at momentum $\mathbf{k}$ and control parameter ε. The length scale is obtained from the scaling function $F(\mathbf{k}, \varepsilon)$ at time-reversal symmetric momenta $\mathbf{k}_0$ as

$$\xi = \left| \frac{1}{\varepsilon} \frac{(\hat{\mathbf{k}}_s \cdot \nabla_{\mathbf{k}})^2 F(\mathbf{k}, \varepsilon)|_{\mathbf{k}=\mathbf{k}_0}}{\partial_\varepsilon F(\mathbf{k}_0, \varepsilon)} \right|^{1/2}. \tag{A2}$$

Using this approach, we obtain the critical exponent ν of the BHZ model: $\nu = 1$ for $c = 0$ and $\nu = 1/2$ for $0 < c \ll 1$.

APPENDIX B: CONSERVATION OF BULK INVARIANTS

By definition, topological invariants do not change during adiabatic transformations of the Hamiltonian that respect the important symmetries. However, more general nonadiabatic transformations during which the band gap can even close were found to preserve the Chern number (at least for two-band

systems) [10,11] too. Below we generalize the proof of the conservation of the Chern number to the case of multiple-band systems, and we give a concise proof of the conservation of the $\mathbb{Z}_2$ invariant.

1. Conservation of the Chern number

For a two-dimensional insulating noninteracting system with translational symmetry one can define the Chern number [53] as

$$C = \frac{1}{2\pi} \sum_{n=1}^{N_F} \int d\mathbf{k} \, \Omega_n(\mathbf{k}), \tag{B1}$$

$$\Omega_n(\mathbf{k}) = -i\, \partial_{k_x} \langle u_n(\mathbf{k})|\partial_{k_y}|u_n(\mathbf{k})\rangle + i\, \partial_{k_y} \langle u_n(\mathbf{k})|\partial_{k_x}|u_n(\mathbf{k})\rangle, \tag{B2}$$

where $\Omega_n(\mathbf{k})$ is the Berry curvature of the nth band.

Let the system be in a state with the Chern number C and the Berry curvature $\Omega_n(\mathbf{k})$ with N_F occupied states $|u_n(\mathbf{k})\rangle$. We limit our discussion to transformations with translational symmetry described by a unitary operator $U(\mathbf{k})$, so each state is transformed as

$$|u_n(\mathbf{k})\rangle \to |u_n'(\mathbf{k})\rangle = U(\mathbf{k})|u_n(\mathbf{k})\rangle. \tag{B3}$$

The Berry curvature after the transformation is

$$\Omega_n'(\mathbf{k}) = -i\, \partial_{k_x} \langle U(\mathbf{k})u_n(\mathbf{k})|\partial_{k_y}|U(\mathbf{k})u_n(\mathbf{k})\rangle$$
$$+ i\, \partial_{k_y} \langle U(\mathbf{k})u_n(\mathbf{k})|\partial_{k_x}|U(\mathbf{k})u_n(\mathbf{k})\rangle$$
$$= \Omega_n(\mathbf{k}) - i\, \partial_{k_x} \langle u_n(\mathbf{k})|U(\mathbf{k})^\dagger \big[\partial_{k_y} U(\mathbf{k})\big]|u_n(\mathbf{k})\rangle$$
$$+ i\, \partial_{k_y} \langle u_n(\mathbf{k})|U(\mathbf{k})^\dagger \big[\partial_{k_x} U(\mathbf{k})\big]|u_n(\mathbf{k})\rangle, \tag{B4}$$

where we used $\partial_{k_i}|U(\mathbf{k})u_n(\mathbf{k})\rangle = [\partial_{k_i} U(\mathbf{k})]|u_n(\mathbf{k})\rangle + U(\mathbf{k})\partial_{k_i}|u_n(\mathbf{k})\rangle$. Note that expressions $\langle u_n(\mathbf{k})|\hat{O}(\mathbf{k})|u_n(\mathbf{k})\rangle = \mathrm{Tr}[\rho_n(\mathbf{k})\hat{O}(\mathbf{k})]$ are smooth in $\mathbf{k}$ when $\hat{O}(\mathbf{k})$ and the density matrix $\rho_n(\mathbf{k}) = |u_n(\mathbf{k})\rangle\langle u_n(\mathbf{k})|$ are smooth in $\mathbf{k}$. When $U(\mathbf{k})$ is smooth in $\mathbf{k}$, which is true for time evolutions with Hamiltonians that are smooth in $\mathbf{k}$, the second and the third terms in $\Omega_n(\mathbf{k})$ are continuous functions of $\mathbf{k}$, and the Chern

number can be written as

$$
C' = C + \frac{1}{2\pi} \sum_{n=1}^{N_F} \int dk_y \int dk_x (-i) \partial_{k_x} \langle u_n(\mathbf{k})| U(\mathbf{k})^\dagger
$$

$$
\times \left[\partial_{k_y} U(\mathbf{k}) \right] |u_n(\mathbf{k})\rangle
$$

$$
+ \frac{1}{2\pi} \sum_{n=1}^{N_F} \int dk_x \int dk_y \, i \, \partial_{k_y} \langle u_n(\mathbf{k})| U(\mathbf{k})^\dagger
$$

$$
\times \left[\partial_{k_x} U(\mathbf{k}) \right] |u_n(\mathbf{k})\rangle. \tag{B5}
$$

Using the periodicity of $U(\mathbf{k})$ and $|u_n(\mathbf{k})\rangle$ over the Brillouin zone, the first integral over k_x, and the second integral over k_y are zero (or, put differently, each component of the vector field $\langle u_n(\mathbf{k})| U(\mathbf{k})^\dagger [\partial_{k_i} U(\mathbf{k})] |u_n(\mathbf{k})\rangle$ is smooth in $\mathbf{k}$, hence the Stokes theorem can be applied). Hence, we obtain $C' = C$, i.e., the Chern number is conserved under a unitary transformation.

To show that our proof reduces to the one for two-band systems performed by D'Allesio and Rigol in Ref. [11], we calculate the time derivative of the Chern number (B5). $U(\mathbf{k})$ now represents the time-evolution operator and by taking into account that $\partial_t U^\dagger(\mathbf{k})[\partial_{k_i} U(\mathbf{k})] = -i U^\dagger(\mathbf{k})[\partial_{k_i} \hat{H}(\mathbf{k})] U(\mathbf{k})$, we get

$$
\partial_t C' = \frac{1}{2\pi} \sum_{n=1}^{N_F} \int d\mathbf{k} \{ \partial_{k_y} \langle u'_n(\mathbf{k})| [\partial_{k_x} \hat{H}(\mathbf{k})] |u'_n(\mathbf{k})\rangle
$$

$$
- \partial_{k_x} \langle u'_n(\mathbf{k})| [\partial_{k_y} \hat{H}(\mathbf{k})] |u'_n(\mathbf{k})\rangle \}. \tag{B6}
$$

For a two-band Hamiltonian $\hat{H}(\mathbf{k}) = -\frac{1}{2}\mathbf{B}(\mathbf{k}) \cdot \hat{\boldsymbol{\sigma}}$ and the state expressed with the density matrix $\hat{\rho}(\mathbf{k}) = \frac{1}{2}[\hat{\sigma}_0 + \mathbf{S}(\mathbf{k}) \cdot \hat{\boldsymbol{\sigma}}]$, we obtain the result from Ref. [11],

$$
\partial_t C' = \frac{1}{4\pi} \int d\mathbf{k} \{ \partial_{k_x} [\mathbf{S}(\mathbf{k}) \cdot \partial_{k_y} \mathbf{B}(\mathbf{k})] - \partial_{k_y} [\mathbf{S}(\mathbf{k}) \cdot \partial_{k_x} \mathbf{B}(\mathbf{k})] \},
$$

$$
\tag{B7}
$$

which vanishes after the application of the Stokes theorem due to the smoothness of $\mathbf{S}(\mathbf{k}) \cdot \partial_{k_i} \mathbf{B}(\mathbf{k})$ at all times.

2. Conservation of the $\mathbb{Z}_2$ invariant

The $\mathbb{Z}_2$ invariant can be defined as [54,55]

$$
(-1)^{N_{\text{bulk}}} = \prod_i \frac{\sqrt{\text{Det}[B(\Lambda_i)]}}{\text{Pf}[B(\Lambda_i)]},
$$

$$
B(\mathbf{k})_{mn} = \langle u_m(-\mathbf{k})| \hat{\mathcal{T}} |u_n(\mathbf{k})\rangle, \tag{B8}
$$

where $B(\mathbf{k})$ is the sewing matrix, the connection between states and their time conjugates, Λ_i's are time-reversal invariant momenta, n and m are indices of N_F occupied states $|u_n(\mathbf{k})\rangle$, and $\text{Pf}[A]$ is the Pfaffian of the matrix A. The formula is valid only when the wave functions are smooth over the whole first Brillouin zone [54]. Such a smooth gauge is possible to construct whenever the Chern number vanishes, which is the case for time-reversal symmetric systems [56].

Let the system initially have a well-defined $\mathbb{Z}_2$ invariant. We again limit the discussion to time evolutions described by unitary transformations that preserve the translational symmetry $U(\mathbf{k})$. Each state is transformed as in Eq. (B3) and the sewing

matrix as

$$
B(\Lambda_i)_{mn} \to B'(\Lambda_i)_{mn} = \langle u_m(\Lambda_i)| U^\dagger(\Lambda_i) \hat{\mathcal{T}} U(\Lambda_i) |u_n(\Lambda_i)\rangle. \tag{B9}
$$

If $U(\Lambda_i)$ commutes with $\hat{\mathcal{T}}$ and $U(\mathbf{k})$ is smooth in $\mathbf{k}$, which is true for time evolutions with Hamiltonians that are time-reversal symmetric and smooth in $\mathbf{k}$, $B'(\Lambda_i) = B(\Lambda_i)$ and $N'_{\text{bulk}} = N_{\text{bulk}}$.

APPENDIX C: PERTURBATIVE EVALUATION OF THE SPIN HALL CONDUCTIVITY

In the main text, we calculated the spin Hall conductivity from the expectation value of the spin current density (7), which we evaluated for a Hamiltonian with an explicitly included electric field. For small electric fields, one can evaluate the spin Hall conductivity also perturbatively. Let the electrons immediately after the quench occupy the states $\{|\varphi_\alpha(\mathbf{k})\rangle = \sum_n c_{\alpha,n}(\mathbf{k})|u_n(\mathbf{k})\rangle, 1 \leqslant \alpha \leqslant N_F\}$ where $|u_n(\mathbf{k})\rangle$'s are the eigenstates of the postquench Hamiltonian $\hat{H}(\mathbf{k})$ without an electric field. The response due to the electric field $E_x(t)$ can be evaluated using the time-dependent perturbation theory as in Ref. [13]. The resulting spin Hall conductivity reads

$$
\sigma_{xy}^{\text{spin}}(t) = \frac{2e}{(2\pi)^2} \text{Re} \sum_\alpha^{N_F} \sum_{n,n'm=1}^{2N_F} \int d\mathbf{k} \, c_{\alpha,n}^*(\mathbf{k}) c_{\alpha,n'}(\mathbf{k}) f_{nn'm}(t,\mathbf{k})
$$

$$
\times \langle u_n(\mathbf{k})| \frac{1}{2}\hat{s}_z \partial_{k_y} \hat{H} |u_m(\mathbf{k})\rangle \langle u_m(\mathbf{k})| \partial_{k_x} \hat{H} |u_{n'}(\mathbf{k})\rangle,
$$

$$
\tag{C1}
$$

$$
f_{nn'm}(t,\mathbf{k}) = -i e^{i\Delta_{nm}(\mathbf{k})t} \int_0^t e^{i\Delta_{mn'}(\mathbf{k})t'} A_x(t') dt' / E_x(t), \tag{C2}
$$

where $\Delta_{nm}(\mathbf{k}) = E_n(\mathbf{k}) - E_m(\mathbf{k})$ and $A_x(t) = -\int E_x(t) dt$. In Eq. (C1) the spin Hall conductivity is expressed with time-independent coefficients of the postquench state $c_{\alpha,n}(\mathbf{k})$, likewise time-independent matrix elements of $\frac{1}{2}\hat{s}_z \partial_{k_y} \hat{H}$ and $\partial_{k_x} \hat{H}$ and a time-dependent function $f_{nn'm}(t,\mathbf{k})$ which is expressed in terms of energies of the states $E_n(\mathbf{k})$ and the dependence of the electric field on time. It turns out that for parameters used in our paper, Eq. (C1) gives results that are essentially the same as that of the full evaluation specified in the main text. A comparison between the results of Eq. (C1) (all) and of the full evaluation (dotted line) is shown in Fig. 8(a).

Expression (C1) is convenient for the interpretation of the results. The contributions to the spin Hall conductivity that include diagonal elements of the density matrix in the basis of Hamiltonian eigenstates $|c_{\alpha,n}(\mathbf{k})|^2$ (hereafter referred to as "diagonal terms"), and contributions including off-diagonal elements of the density matrix $c_{\alpha,n}^*(\mathbf{k}) c_{\alpha,n'}(\mathbf{k})$ (referred to as "off-diagonal terms") behave differently, see Fig. 8(a). One can see that the diagonal terms give rise to the finite average value of $\sigma_{xy}^{\text{spin}}$. The frequency of the decaying small oscillations around this average value is given by the magnitude of the gap. The off-diagonal terms, on the other hand, exhibit oscillations around 0 with the magnitude that for long times increases in time quadratically. The observed time dependence can
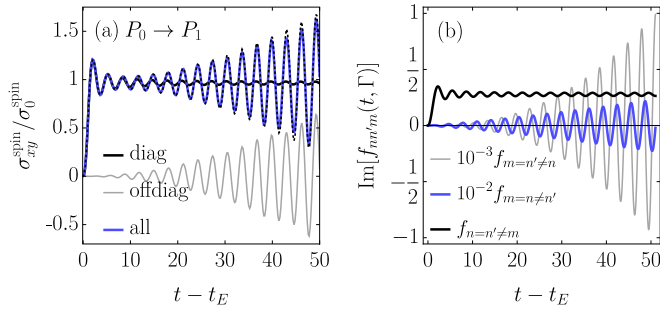
FIG. 8. (a) Diagonal (diag), off-diagonal (offdiag), all terms (all) in $\sigma_{xy}^{\mathrm{spin}}(t)$ according to Eq. (C1), and $\sigma_{xy}^{\mathrm{spin}}(t)$ resulting from the full evaluation of Eq. (7) (dotted) for the system after the $P_0 \to P_1$ quench for $\tau_u = 15$. (b) Imaginary part of the time-dependent element $f_{nn'm}(t,\Gamma)$ at the Γ point for the system at parameters P_1 is shown for different index combinations. In both figures the electric field is turned on as $E_x(t) = E_0\{1 - \exp[-(t - t_E)/\tau_E]\}$.

be considered analytically by evaluating the time-dependent function $f_{nn'm}(t,\mathbf{k})$.

The diagonal terms contain $\langle u_n(\mathbf{k})|\frac{1}{2}\hat{s}_z\partial_{k_y}\hat{H}|u_m(\mathbf{k})\rangle\langle u_m(\mathbf{k})|\partial_{k_x}\hat{H}|u_n(\mathbf{k})\rangle$, which is nonvanishing only for index combinations $n \neq m$ where it is imaginary. Therefore, only the imaginary part of the function $f_{nnm}(t,\mathbf{k})$ contributes to the

integral. The explicit evaluation for long times ($t \gg \tau_E$) yields $\mathrm{Im}[f_{nnm}(t,\mathbf{k})]$

$$= \frac{1}{\Delta_{nm}^2(\mathbf{k})} - \frac{\cos[\Delta_{nm}(\mathbf{k})t] + \Delta_{nm}(\mathbf{k})\tau_E \sin[\Delta_{nm}(\mathbf{k})t]}{\Delta_{nm}(\mathbf{k})^2[1 + \Delta_{nm}^2(\mathbf{k})\tau_E^2]}. \quad \text{(C3)}$$

For long times, the function at every $\mathbf{k}$ oscillates around a finite mean value $1/\Delta_{nm}(\mathbf{k})^2$. The amplitude of oscillations vanishes with $\tau_E \to \infty$.

We now turn to the off-diagonal terms. The leading off-diagonal terms are given by index combinations $m = n' \neq n$, and the corresponding time-dependent function for long times grows quadratically with t, $f_{nmm}(t,\mathbf{k}) = i\, e^{-i\Delta_{nm}(\mathbf{k})t}[(t - \tau_E)^2 + \tau_E^2]/2$. Other off-diagonal index combinations give rise to oscillations that grow linearly with time and are hence important only initially. Figure 8(b) shows the imaginary part of the function $f_{nn'm}(t,\mathbf{k})$ for different index combinations.

Finally, we note that, in the limit of an infinitely slow quench, excitations are present with probability 1 only at $\mathbf{k}$ where the band gap closes. For such a system, the off-diagonal elements of the density-matrix $c_{\alpha,n}^*(\mathbf{k})c_{\alpha,n'}(\mathbf{k})$ are equal to zero for every $\mathbf{k}$, meaning that the growth of oscillations never occurs and the spin Hall response is equal to the ground-state one.

[1] A. R. Mellnik, J. S. Lee, A. Richardella, J. L. Grab, P. J. Mintun, M. H. Fischer, A. Vaezi, A. Manchon, E.-A. Kim, N. Samarth, and D. C. Ralph, Nature (London) **511**, 449 (2014).

[2] Y. Fan, P. Upadhyaya, X. Kou, M. Lang, S. Takei, Z. Wang, J. Tang, L. He, L.-T. Chang, M. Montazeri, G. Yu, W. Jiang, T. Nie, R. N. Schwartz, Y. Tserkovnyak, and K. L. Wang, Nature Mater. **13**, 699 (2014).

[3] N. Xu, Y. Xu, and J. Zhu, npj Quantum Materials **2**, 51 (2017).

[4] G. Gupta, M. B. A. Jalil, and G. Liang, Sci. Rep. **4**, 6838 (2014).

[5] W. Tian, W. Yu, J. Shi, and Y. Wang, Materials **10**, 814 (2017).

[6] K. v. Klitzing, G. Dorda, and M. Pepper, Phys. Rev. Lett. **45**, 494 (1980).

[7] R. B. Laughlin, Phys. Rev. B **23**, 5632 (1981).

[8] D. J. Thouless, M. Kohmoto, M. P. Nightingale, and M. den Nijs, Phys. Rev. Lett. **49**, 405 (1982).

[9] C. L. Kane and E. J. Mele, Phys. Rev. Lett. **95**, 146802 (2005).

[10] M. S. Foster, M. Dzero, V. Gurarie, and E. A. Yuzbashyan, Phys. Rev. B **88**, 104511 (2013).

[11] L. D'Alessio and M. Rigol, Nat. Commun. **6**, 8336 (2015).

[12] M. D. Caio, N. R. Cooper, and M. J. Bhaseen, Phys. Rev. Lett. **115**, 236403 (2015).

[13] M. D. Caio, N. R. Cooper, and M. J. Bhaseen, Phys. Rev. B **94**, 155104 (2016).

[14] J. H. Wilson, J. C. W. Song, and G. Refael, Phys. Rev. Lett. **117**, 235302 (2016).

[15] P. Wang and S. Kehrein, New J. Phys. **18**, 053003 (2016).

[16] P. Wang, M. Schmitt, and S. Kehrein, Phys. Rev. B **93**, 085134 (2016).

[17] U. Bhattacharya, J. Hutchinson, and A. Dutta, Phys. Rev. B **95**, 144304 (2017).

[18] Y. Hu, P. Zoller, and J. C. Budich, Phys. Rev. Lett. **117**, 126803 (2016).

[19] F. N. Ünal, E. J. Mueller, and M. O. Oktel, Phys. Rev. A **94**, 053604 (2016).

[20] M. Schüler and P. Werner, Phys. Rev. B **96**, 155122 (2017).

[21] A. Bermudez, L. Amico, and M. A. Martin-Delgado, New J. Phys. **12**, 055014 (2010).

[22] W. DeGottardi, D. Sen, and S. Vishveshwara, New J. Phys. **13**, 065028 (2011).

[23] P. D. Sacramento, Phys. Rev. E **90**, 032138 (2014).

[24] T. W. B. Kibble, J. Phys. A **9**, 1387 (1976).

[25] W. H. Zurek, Nature (London) **317**, 505 (1985).

[26] A. Dutta, R. R. P. Singh, and U. Divakaran, Europhys. Lett. **89**, 67001 (2010).

[27] L. Privitera and G. E. Santoro, Phys. Rev. B **93**, 241406 (2016).

[28] B. A. Bernevig, T. L. Hughes, and S.-C. Zhang, Science **314**, 1757 (2006).

[29] W. S. König, Markus, C. Brüne, A. Roth, H. Buhmann, L. W. Molenkamp, X.-L. Qi, and S.-C. Zhang, Science **318**, 766 (2007).

[30] C. Liu, T. L. Hughes, X.-L. Qi, K. Wang, and S.-C. Zhang, Phys. Rev. Lett. **100**, 236601 (2008).

[31] I. Knez, R.-R. Du, and G. Sullivan, Phys. Rev. Lett. **107**, 136603 (2011).

[32] F. Reis, G. Li, L. Dudy, M. Bauernfeind, S. Glass, W. Hanke, R. Thomale, J. Schäfer, and R. Claessen, Science **357**, 287 (2017).

[33] S. Wu, V. Fatemi, Q. D. Gibson, K. Watanabe, T. Taniguchi, R. J. Cava, and P. Jarillo-Herrero, Science **359**, 76 (2018).

[34] Y. Yao and Z. Fang, Phys. Rev. Lett. **95**, 156601 (2005).

[35] R. Yu, X. L. Qi, A. Bernevig, Z. Fang, and X. Dai, Phys. Rev. B **84**, 075119 (2011).

[36] J. K. Asbóth, L. Oroszlány, and A. Pályi, *A Short Course on Topological Insulators* (Springer International Publishing, Switzerland, 2016).

[37] C. L. Kane and E. J. Mele, Phys. Rev. Lett. **95**, 226801 (2005).

[38] S. Murakami, N. Nagaosa, and S.-C. Zhang, Phys. Rev. B **69**, 235206 (2004).

[39] J. Shi, P. Zhang, D. Xiao, and Q. Niu, Phys. Rev. Lett. **96**, 076604 (2006).

[40] C. Gorini, R. Raimondi, and P. Schwab, Phys. Rev. Lett. **109**, 246604 (2012).

[41] C. Zener, Proc. R. Soc. London, Ser. A **137**, 696 (1932).

[42] W. Chen, M. Sigrist, and A. P. Schnyder, J. Phys.: Condens. Matter **28**, 365501 (2016).

[43] M. Rigol, V. Dunjko, and M. Olshanii, Nature (London) **452**, 854 (2008).

[44] L. Vidmar and M. Rigol, J. Stat. Mech.: Theory Exp. (2016), 064007.

[45] D. G. Rothe, R. W. Reinthaler, C.-X. Liu, L. W. Molenkamp, S.-C. Zhang, and E. M. Hankiewicz, New J. Phys. **12**, 065012 (2010).

[46] D. Xiao, W. Zhu, Y. Ran, N. Nagaosa, and S. Okamoto, Nat. Commun. **2**, 596 (2011).

[47] J. Wang, B. Lian, and S.-C. Zhang, Phys. Rev. Lett. **115**, 036805 (2015).

[48] M. Aidelsburger, M. Atala, M. Lohse, J. T. Barreiro, B. Paredes, and I. Bloch, Phys. Rev. Lett. **111**, 185301 (2013).

[49] H. Miyake, G. A. Siviloglou, C. J. Kennedy, W. C. Burton, and W. Ketterle, Phys. Rev. Lett. **111**, 185302 (2013).

[50] G. Jotzu, M. Messer, R. Desbuquois, M. Lebrat, T. Uehlinger, D. Greif, and T. Esslinger, Nature (London) **515**, 237 (2014).

[51] M. Aidelsburger, M. Lohse, C. Schweizer, M. Atala, J. Barreiro, S. Nascimbéne, N. Cooper, I. Bloch, and N. Goldman, Nat. Phys. **11**, 162 (2015).

[52] N. Fläschner, B. S. Rem, M. Tarnowski, D. Vogel, D.-S. Lühmann, K. Sengstock, and C. Weitenberg, Science **352**, 1091 (2016).

[53] M. V. Berry and F. R. S., Proc. R. Soc. London, Ser. A **392**, 45 (1984).

[54] L. Fu and C. L. Kane, Phys. Rev. B **74**, 195312 (2006).

[55] B. A. Bernevig and T. L. Hughes, *Topological Insulators and Topological Superconductors* (Princeton University Press, Princeton and Oxford, 2013).

[56] A. A. Soluyanov and D. Vanderbilt, Phys. Rev. B **85**, 115415 (2012).